2023

Numerical Simulation of the Donor-Assisted Stir Material for Friction Stir Welding of Aluminum Alloys and Carbon Steel

Joseph Maniscalco
Old Dominion University

Abdelmageed A. Elmustafa
Old Dominion University

Srinivasa Bhukya

Zhenhua Wu

Original Publication Citation

Maniscalco, J., Elmustafa, A. A., Bhukya, S., & Wu, Z. (2023). Numerical simulation of the donor-assisted stir material for friction stir welding of aluminum alloys and carbon steel. *Metals*, *13*(1), 1-15, Article 164. https://doi.org/10.3390/met13010164

metals

MDPI

Article

Numerical Simulation of the Donor-Assisted Stir Material for Friction Stir Welding of Aluminum Alloys and Carbon Steel

Joseph Maniscalco [1,2], Abdelmageed A. Elmustafa [1,2,*], Srinivasa Bhukya [3] and Zhenhua Wu [3]

[1] Department of Mechanical and Aerospace Engineering, Old Dominion University, Norfolk, VA 23529, USA
[2] The Applied Research Center-Thomas Jefferson National Accelerator Facility, Newport News, VA 23606, USA
[3] Department of Engineering, Virginia State University, Petersburg, VA 23806, USA
* Correspondence: aelmusta@odu.edu

Abstract: In this research effort, we explore the use of a donor material to help heat workpieces without wearing the tool or adding more heat than necessary to the system. The donor material would typically be a small piece (or pieces) of material, presumably of lower strength than the workpiece but with a comparable melting point. The donor, a sandwich material, is positioned between the tool head and the material to be welded, where the tool initially plunges and heats up in the same manner as the parent material that is intended for welding. The donor material heats up subsequent to tool penetration due to friction and as a result heats up the material beneath it. This preheating technique softens the harder parent material, which helps to minimize tool wear and produce better weld performance. The goal is to investigate the use of the donor material as a preheating technique that minimizes wear and tear on the tool head without negatively impacting the structural properties of the weld. To demonstrate the donor material concept, a combination of Cu-Al, Cu-1045 Carbon steel (CS), and Al-1045 CS sets of donor and parent materials were used in the simulation, in addition to control samples Al-Al and CS-CS. We simulated two thicknesses of donor material 25 and 50% of the parent material thickness, respectively. The simulation suggests that the donor material concept generates phenomenal results by reducing the temperature and axial forces for the friction stir welding of aluminum AA6061 and carbon steel 1045. It also assists downstream during welding, resulting from frictional mechanical work which is converted into stored heat.

Keywords: friction stir welding; donor material; material processing

Citation: Maniscalco, J.; Elmustafa, A.A.; Bhukya, S.; Wu, Z. Numerical Simulation of the Donor-Assisted Stir Material for Friction Stir Welding of Aluminum Alloys and Carbon Steel. *Metals* **2023**, *13*, 164. https://doi.org/10.3390/met13010164

Academic Editor: Tomasz Kik

Received: 15 December 2022
Revised: 3 January 2023
Accepted: 9 January 2023
Published: 13 January 2023

1. Introduction

Friction stir welding (FSW) is a relatively simple process by which a spinning tool head plunges into two adjacent workpieces [1,2]. Scientists have continuously developed various techniques to improve aspects of the friction stir welding of dissimilar materials [3–8]. A tool head establishes contact with the material intended for welding, resulting in generating frictional forces. These frictional forces create enough heat to plastically deform the material and enable it to be moved along the joint line to weld the workpieces together in the solid phase. FSW has been used successfully in the industry to weld aluminum and thin metal sheets. It has also been popular in heavy industries such as aerospace and shipbuilding. The wear on the tool head has limited the use of FSW for long weld lines and deep weld penetrations [9,10]. The process of FSW mainly consists of three stages: plunge, dwell, and welding stages. In the plunge stage, a high hardness non-consumable rotating tool penetrates the plates intended for welding. In the dwell stage, the tool head penetrates the metal and rotates, whereas the welding stage is the stage which, upon completion, will result in a final welded plate [1,11–15]. The plunge and welding stages in FSW processes are particularly significant since most of the elastic/plastic/thermomechanical deformations and the material experiences phase transformation occur due to the excessive heat and stresses generated during deformation in the plunge stage. Study of the highly dynamic

plunge stage is challenging due to excess deformations and high strain rates resulting from the tool head piercing the test specimen. Increasingly, it is becoming of great interest to successfully friction stir weld high-strength alloys such as steel and titanium-based alloys. This process requires a methodical understanding of the plunge stage [16–18]. Experimental and numerical research are increasingly becoming imperative to investigate material processes during these two stages. There are few investigations that focus on the welding stage [19–22], and not many experimental or numerical studies focus on the excessive deformation caused by the thermo-mechanical nature of the plunge and welding phases. Some FEM-based numerical modeling simulate either the welding stage [23] or the dwell and the welding stages [24], but not the plunge and the welding stages. Khosa (2010) constructed a physically based coupled thermomechanical model to investigate FSW and friction stir spot welding (FSSW) during the plunge stage [25]. The numerical simulation of the plunge stage is hindered by the excessive mesh distortion which often results in the premature termination of the program [26].

Guerdoux and Fourment used Forge3D modeling software to model all phases of FSW, utilizing an arbitrary Lagrangian–Eulerian (ALE) built-in formulation. They concluded that the modeling of the resulting forces could be possible once the contact conditions between the tool head and the workpiece are calibrated and identified [27]. They also concluded that preliminary comparisons between the simulations and experimental results indicated that the numerical model was able to replicate the chief phenomena occurring in FSW [27]. Tool temperature profile and forces were accurately captured at a steady welding state, for different welding speeds, using Forge3D simulation software by Assidi et al. [28]. The numerical simulations used an arbitrary Lagrangian–Eulerian (ALE) formulation. Hossfeld used the coupled Eulerian–Lagrangian (CEL) formulation in Abaqus/Explicit to simulate FSW of two separate plates mimicking actual tool geometries [29–31]. Hossfeld also concluded that the ALE and CEL approaches are competitively similar and computationally intensive depending on the level of detail, requiring up to several days of computational time to complete a few seconds of the complex FSW process [29,31]. Bagheri et al. used smoothed particle hydrodynamics (SPH) and graphics processing units (GPUs) to investigate the temperature history, strain, and stress distributions during conventional as well as submerged FSW (SFSW) [25]. In addition to the coupled thermo-mechanical simulation models, pure CFD models were successfully used to model actual FSW tool geometries. These investigations generally focus only on the analysis of the steady state of the process during the welding stage [26,32,33]. Hossfeld elucidated that using CFD, it is difficult to simulate the entire FSW process, i.e., the plunge, dwell, and welding stages, in a single continuous simulation model due to systematic constraints and the complexity of the problem [20]. In this study, we explore a donor material which is to be positioned between the tool head and the workpiece to assist in heating the workpiece without causing severe wearing of the tool head or adding more heat than necessary to the system. The donor material would typically be a small piece (or pieces) of material, one that presumably is of lower strength than the workpiece but that has a comparable melting point. The donor material heats up after tool penetration due to friction and subsequently heats the material beneath it. This preheating technique softens the high-strength parent material, helping to minimize tool wear and produce better weld performance. Our goal is to investigate the use of the donor material as a preheating technique that minimizes wear and tear on the tool head without negatively impacting the structural properties of the weld.

2. Simulation Motivation

To mitigate the severe wear and tear conditions of the FSW tool head due to contact friction between the tool head and the material to be welded, we demonstrate use of the donor material concept introduced by [18,26–32]. The donor material concept, which is heat management, focuses on understanding the fundamental interface mechanisms that influence interactions between the tool pin, tool shoulder, and surrounding material flow in the workpiece. A donor material whose hardness and melting point are relatively lower

than the counterparts of the workpieces is selected first before starting the FSW process. A groove is prepared at the beginning of the weld line to hold the insert of the donor material. Before beginning the welding process, first, the tool pin spins and plunges into the softer donor material. This plunging process generates a plastic work zone with a plastic flow surrounding the tool. We hypothesize that the plastic work zone stays with the tool pin and serves as a pre-heating mechanism that can soften the nearby material of the workpieces ahead of the tool pin during plunging and traveling. This plastic flow can shield from the contact friction between the tool surface and the high-strength workpieces. Thus, once the plastic zone is established, the combination of preheating and plastic flow reduces the amount of energy and the frictional forces required to advance the tool pin. We aim to understand better the thermo-mechanical mechanisms involved in creating the plastic work zone and the resulting heat generated from the process. The proposed efforts specifically involve numerical modeling of the entire FSW process, plunge, and weld stages, analyzing the plastic zone, and studying the resulting heat distribution throughout the workpiece. To demonstrate the donor material concept, a combination of Cu-Al, Cu-1045 Carbon steel (CS), and Al-1045 CS sets of donor and parent materials were used in the simulation in addition to controling samples Al-Al, and CS-CS. Table 1 lists the donor–workpiece material combinations, and Table 2 lists their corresponding properties. The donor material is quoted first followed by a hyphenate, and then the material to be welded (parent material) next, i.e., for Cu-Al, Cu is the donor material while Al is the parent material. We simulated two thicknesses of donor material, 25% and 50% of the parent material thickness, respectively.

Table 1. Donor–workpiece combinations.

Material Combination	Donor	Workpiece	Abbreviations	Notes
Aluminum–aluminum	No donor	Aluminum	Al-Al	Control samples
1045 carbon steel–1045 carbon steel	No donor	1045 carbon steel	CS-CS	Control samples
Copper–aluminum	Copper	Aluminum	Cu-Al	Donor–workpiece
Copper–1045 carbon steel	Copper	1045 carbon steel	CS	Donor–workpiece
Aluminum–1045 carbon steel	Aluminum	1045 carbon steel	Al-CS	Donor–workpiece

Table 2. Temperature-dependent material properties for Al2024-T3, Cu, and 1045 mild steel.

Material	Thermal Conductivity [W/mK]	Density [kg/m^3]	E [GPa]	v	Inelastic Heat Fraction	Specific Heat [J/kg °C]
Al2024-T3 [33]	121	2770	73	0.34	0.9	875
Cu [34]	386	8960	124	0.34	0.9	383
1045 Steel [35]	49.8	7850	205	0.29	0.9	486

3. Material Modeling

The selection of an appropriate constitutive law to reflect the interaction of flow stress with temperature, plastic strain and strain rate is essential for modeling the FSW process. For this reason, the temperature- and strain rate-dependent elastic-plastic Johnson-Cook law is selected for this model. The constitutive law in this case, calculates the flow stress as a function of temperature and strain rate up to the melting point or solidus temperature. For Al 2024, the solidus temperature is set to 502 °C. Johnson-Cook is a thermomechanical

constitutive model which integrates temperature and stresses with friction control. The Johnson–Cook constitutive law is given by:

$$\overline{\sigma} = \left[A + B\left(\overline{\epsilon}^{pl}\right)^{n}\right]\left[1 + C\, ln\left(\frac{\dot{\overline{\epsilon}}^{pl}}{\dot{\epsilon}_0}\right)\right]\left(1 - \hat{\theta}^{m}\right), \quad (1)$$

and

$$\dot{\overline{\epsilon}}^{pl} = \dot{\epsilon}_0 e^{\left(\frac{1}{C}(R-1)\right)} \text{ for } \overline{\sigma} \geq \sigma^0, \quad (2)$$

$\hat{\theta}$ is the nondimensional temperature defined as

$$\hat{\theta} = \begin{cases} 0 & for\ \theta < \theta_{transition} \\ (\theta - \theta_{transition})/\left(\theta_{melting} - \theta_{transition}\right) & for\ \theta_{transition} \leq \theta \leq \theta_{melting} \\ 1 & for\ \theta > \theta_{melting} \end{cases} \quad (3)$$

$\overline{\sigma}$ is yield stress at nonzero strain rate; $\dot{\overline{\epsilon}}^{pl}$ is the equivalent plastic strain rate; $\dot{\epsilon}_0$ and C are material parameters measured at or below the transition temperature, $\theta_{transition}$; $\sigma^0\left(\dot{\overline{\epsilon}}^{pl}, \theta\right)$ is the static yield stress; $R\left(\dot{\overline{\epsilon}}^{pl}\right)$ is the ratio of the yield stress at nonzero strain rate to the static yield stress; $\hat{\theta}$ is the nondimensional temperature, defined as a function of the melting and the transition temperatures, θ_{melt} and $\theta_{transition}$. A, B, C, n, and m are material parameters that are measured at or below the transition temperature. The material parameters for Al 2024-T3 are adapted from Schmidt and Hattel (2005) [33]. The Johnson-Cook model material parameter are listed in Table 3.

Table 3. Johnson–Cook Rate Dependent parameters.

Material	A [MPa]	B [MPa]	C	n	m	Solidus Temp. [°C]	Transition Temp. [°C]	$\dot{\epsilon}$
Al2024-T3	369	684	0.0083	0.73	1.7	502	25	1
Cu	90	292	0.025	0.31	1.09	1083	25	1
1045 Steel	553	601	0.013	0.234	1	1440	25	1

4. Simulation Details

The numerical modeling of FSW poses a challenge due to the high strain rates and temperatures involved in the process, resulting in a complicated problem involving non-linear material behavior. Simulation of the entire FSW process was performed using an elasto-plastic constitutive law, available in Abaqus finite element code [36]. Abaqus possesses the capabilities of handling non-linear problems, and we adopt the built-in Johnson-Cook material law in the present simulation. Abaqus explicit solver, combined with the coupled Eulerian–Lagrangian (CEL) formulation, is used in modeling of the FSW problems posed in this research. The model consists of a deformable workpiece and a rigid stir welding tool to ensure that all generated heat from friction will transfer properly to the bottom workpiece through the Cu donor material, provided that no heat will escape to the tool head. The deformable workpiece dimensions are 100 mm × 100 mm × 20 mm, and the donor material dimensions are 15 mm × 15 mm × 5 mm for the 25% donor and 15 mm × 15 mm × 10 mm for the 50% donor. The rigid stir welding tool has a 30 mm diameter. The pin has the same height and diameter dimensions, those being 10 mm and a 7° taper angle, respectively.

The workpiece is meshed using 8-node coupled temperature displacement brick elements (C3D8RT). The mesh is graded with higher mesh density around the tool plunge area. This meshing scheme improves the accuracy of the solution around the tool without tremendously increasing the computational time. The graded meshes are obtained by

partitioning the workpiece into smaller cells. We tried different mesh densities before arriving at the final model. We constrained the bottom surface of the workpiece to prevent bending. We also constrained the sides such that there would be no deformation along the boundary other than compression along the tool plunge direction. The tool is considered a rigid surface with no thermal degrees of freedom and is modeled as a master surface, whereas the workpiece is a slave in terms of the contact conditions between the two surfaces. Friction coefficients, μ of 0.3, 0.5, 0.7, and 1.0 between the tool and the workpiece are used [33], and the penalty contact method is adopted to model the contact interaction between the two surfaces. The Coulomb friction law is used in most of the proposed computational solid mechanics-based finite element packages. In these models, constant or limited ranges for the friction coefficient are employed because the Coulomb friction model is based on the sliding condition [23]. Due to the usage of the constant values for the friction coefficient [23,37,38], the Coulomb friction model is limited to the sliding frictional condition in which the temperature values are low [24]. Frigaard et al. [39] suggested that the friction coefficient between an aluminum plate and a mild steel tool should be between 0.5 for sticking friction and 0.25 for dry sliding, while Soundararajan et al. [40] varied μ between 0.4 and 0.5 according to the welding conditions, and that Schmidt and Hattel [33] used a constant value of μ equal to 0.3. Based on computational solid mechanics modeling, Jl, S.-d., LIU et al. [41] employed the Coulomb friction law in a DEFORM-3D finite element package for modeling the inertia welding process. Nimesh et al. used the Coulomb friction model for modeling dissimilar inertia welding [42]. In the current Abaqus software-based environment simulation, constant values of coefficients of friction of the Coulomb model of 0.3, 0.5, 0.7, and 1.0 were assumed using the refined mesh model. The current simulation involved a tool with a rotational speed of 1400 rpm and a tool with a plunge/weld velocity of 3 mm/s. The simulation results are shown during the plunge and the welding processes for the Al and 1045 CS plates with no donor material, and subsequent to the placement and engagement of the Cu donor material for the Al plate and Cu and Al donor materials for the 1045 CS plate. The simulation results include temperatures and axial forces during the plunge and the welding processes [43]. Figure 1 identifies a full model and a cross section of the donor and parent material regions.

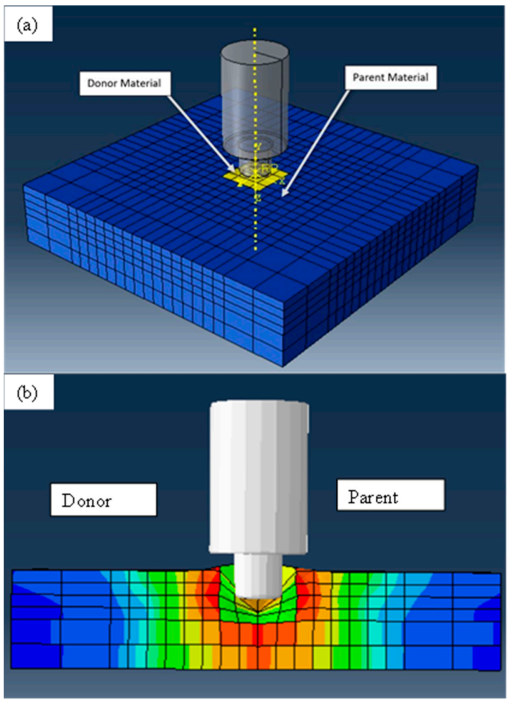

Figure 1. (**a**) Full model of the donor–parent material. (**b**) Cross section of the donor-parent materials combination. The colored map represents temperature distribution in the cross section.

5. Simulation Results

The simulation results are presented for the four separate regions identified in Figure 2 for 25% and 50% donor material. Initially, the model was constructed using 2000 elements. Each element within the donor material region was further dissected into 8 additional elements, resulting in a total of 19,200 total elements. The mesh for the 2000 elements is labeled as coarse mesh and the one for the 19,200 elements as fine mesh. The simulations were performed on the Old Dominion University high-performance computing cluster at first and later, when it was found that there is no advantage or time savings gained by using the cluster, the simulations were performed on desktop and laptop computers with faster processors. On average, the simulations for the coarse mesh took a day and a half to complete, whereas the ones for the fine mesh lasted between 14 and 18 days. In some cases, when we used a higher coefficient of friction, the simulations lasted for longer than 20 days.

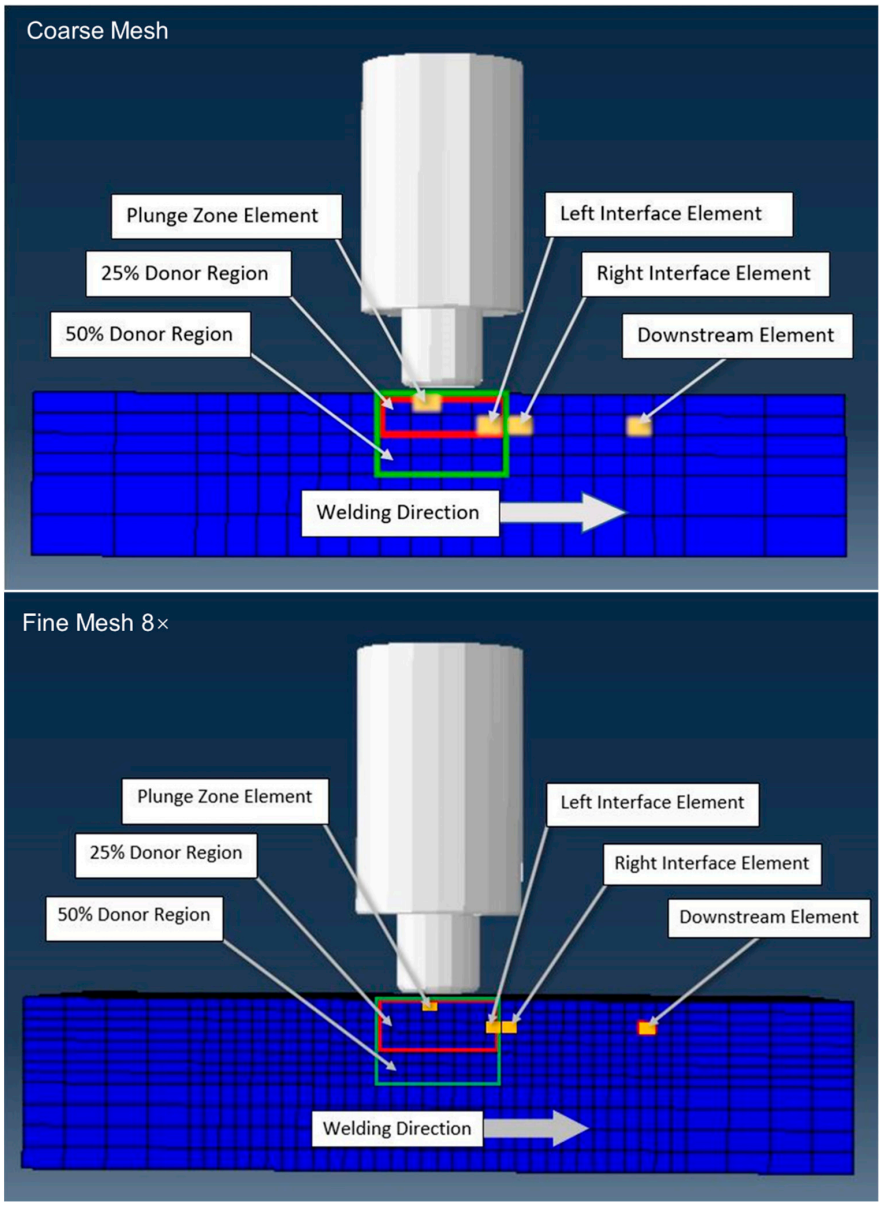

Figure 2. Cross section of the donor and parent materials combination for coarse and fine meshes.

The regions include elements that represent the donor material in the plunge zone, region 1, elements in the donor material which are adjacent to elements in the parent material and which are denoted by the left interface (LI), region 2, elements in the parent

material which are also adjacent to the element in the donor material and which are denoted by the right interface (RI), region 3, and elements in the parent material which are denoted by down-stream (DS), region 4, as shown in Figure 2. The temperature increases from 0 until it reaches 247 °C when plunging into the Al plate with no donor material for 3 s, whereas the temperature after the placement of 25% Cu donor material reaches 88 °C at the end of the 3 s plunge time, Figure 3.

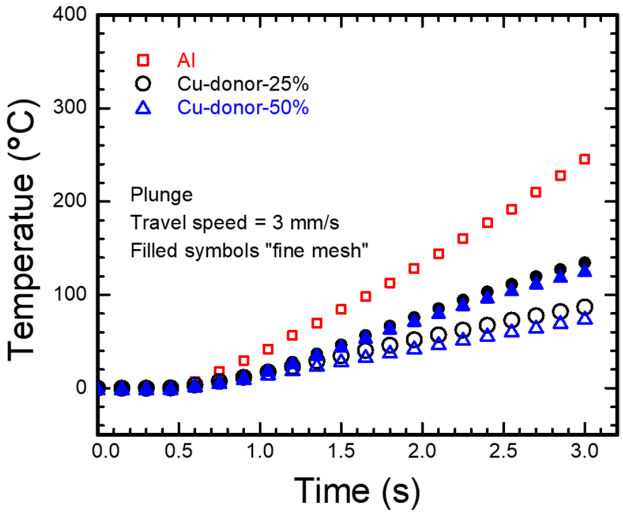

Figure 3. Temperature profile for the 25 and 50% Cu-Al donor/parent material in the plunge zone, region 1.

The 50% donor material reduced the temperature even more, to 72 °C. The Cu donor material has significantly reduced the temperatures in the Al plate from 247 °C to 82 °C, and 250 °C to 72 °C for the 25 and 50% Cu donor material, respectively, during the plunge stage where it is believed that most of the severe plastic deformation takes place, an essential outcome of the donor stir material concept. Similar results were also observed for temperature during the welding stage. The temperature for the fine mesh reaches 133 and 123 °C for the 25% and 50% Cu donor materials, as indicated by the filled symbols in Figure 3.

Similarly, for the 1045 steel plate with no donor material, the temperature increases to 330 °C at the end of the plunge zone, region 1, whereas the temperature after the placement of the 25 and 50% Al donor materials on the 1045 steel plate reaches similar levels at the end of the plunge, 318 and 286 °C, respectively. However, the temperature reaches 118 °C upon the placement of the 25 and 50% Cu donor material on the 1045 steel plate, Figure 4.

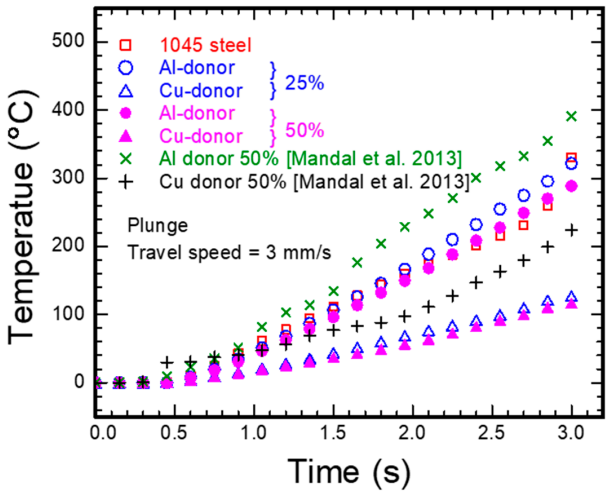

Figure 4. Temperature profile for the 25 and 50% Cu and Al donors on 1045 Steel parent material in the plunge zone, region 1.

It is obvious that plunging into the 25 and 50% Cu donor material reduced the temperature by 64% and 70% in Al plate, respectively. It is also noted that plunging in the 25 and 50% Cu donor material placed on the 1045 steel plate reduced the temperature by 64%, whereas plunging into the Al donor material had no significant impact on the 1045 steel plate. The thickness of the Al donor material also had no impact on the 1045 steel plate and the thickness of the Cu donor material produced similar results for both the Al and the 1045 steel parent materials during the plunge zone, region 1. We later discovered that the donor material thickness significantly impacted the results during the welding process, at LI, RI, and DS, in regions 2,3, and 4, respectively. Since the Cu donor material for both the Al and the 1045 steel plate reduced the temperature by more than 60%, it is expected that this temperature reduction will also impact the tool wear and tear, an advantage of using the donor material. Data from Mandal et al., 2013, in Figure 4 correlate well with the data in the current study [26]. Next, we investigated the temperature results in regions 2, 3, and 4, Figure 5. The temperature for the Al plate with no donor material in regions 2 and 3 reached a maximum of 449 °C at the end of the welding process, i.e., at 11 s. As expected, the temperature for DS, region 4 cooled down to 214 °C.

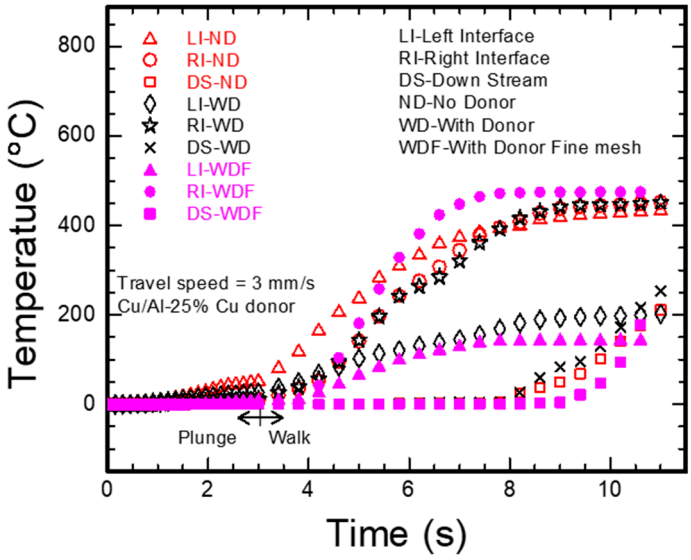

Figure 5. Temperature versus time. The red symbols represent the Al plate with no donor material. LI, region 2 represents 25% Cu donor material on the Al parent material, RI, region 3 represents the Al parent material, and DS, region 4 represents the Al parent material.

Similar results were obtained for the 25% Cu donor material placed on the Al plate for region 2, LI, and region 4, DS. However, the temperature in the Al plate with the donor material, RI, region 3 is identical to the temperature in the Al plate with no donor material. at the end of the welding process, i.e., at 11 s. This is an unexpected result, as we anticipate the temperature in the Al plate after the placement of the Cu donor material to fall to levels below 449 °C It is suspected that, since the specific heat of the Al plate is higher than the specific heat of the Cu donor material, this resulted in higher temperatures in the Al plate.

The results of the fine mesh for the 25% Cu donor material are consistent with the results of the coarse mesh in the three regions, LI, RI, and DS, as show Figure 5. This result indicates that there is no advantage or gain in further refining the mesh for the 25% Cu donor material. The results of Figure 6 are consistent with the concept of the Cu (donor)/Al (parent material) as expected. This difference is due to the Cu donor material of Figure 6 being 50% of the Al parent material compared to the donor Cu material of Figure 5, which is 25% of the Al parent material. Likewise, for the 50% Cu donor material, the results of the fine mesh indicated similar behavior to that of the 25% Cu donor material.

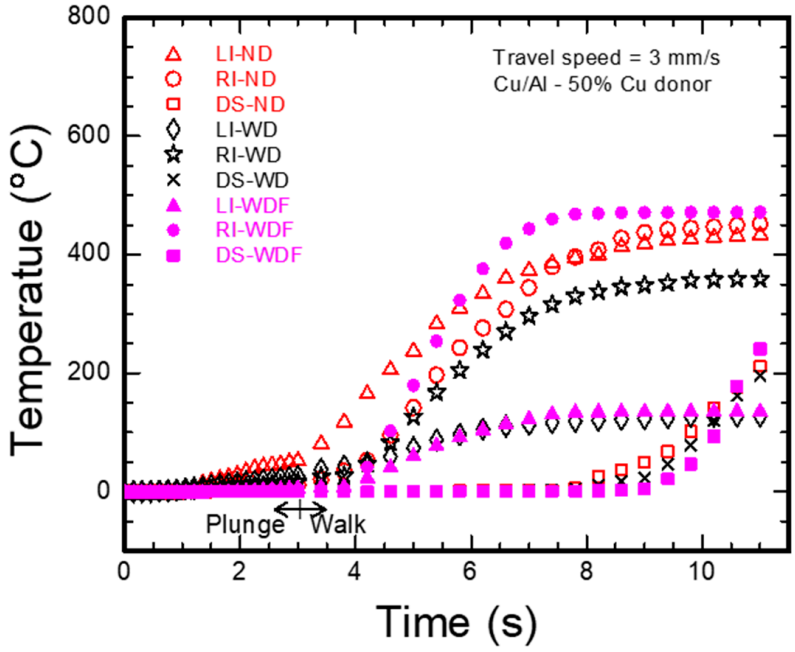

Figure 6. Temperature versus time. The red symbols represent the Al plate with no donor material. LI, region 2 represents 50% Cu donor material on the Al parent material, RI, region 3 represents the Al parent material, and DS, region 4 represents the Al parent material.

A contour plot of the von Mises stresses of the 1400 rpm and 3 mm/s travel speed fine meshes for the 25% (left image) and 50% (right image) Cu donor/Al base materials is shown in Figure 7. The stress distribution covers a wide range in the 50% Cu donor material compared to the 25% Cu donor material.

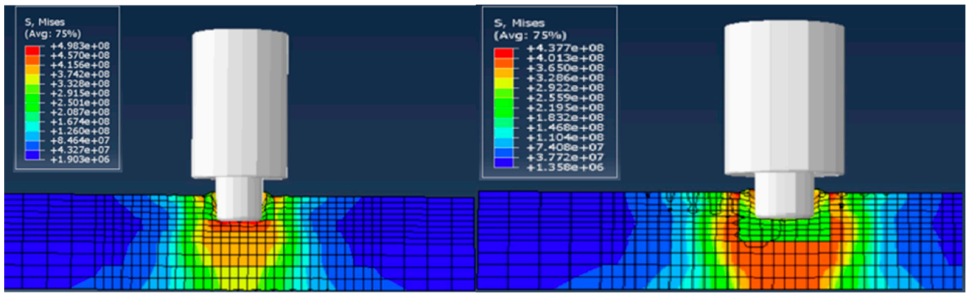

Figure 7. von Mises stress [Pa] distribution of the 1400 rpm and 3 mm/s travel speed fine meshes for 25% (left image) and 50% (right image) Cu donor material/Al base material.

The temperature in the 1045 steel with no donor material for the LI, region 2, and the RI, region 3 at the end of the welding process, i.e., at the end of 11 s is 480 °C, Figure 8. The temperature in the 1045 steel plate in the presence of the Al donor material for the LI at 11 s is similar to the temperature in the 1045 steel with no donor material. Different results were observed for the 1045 steel with Cu donor material, i.e., the temperature in the RI, region 3 is higher at 11 s and reaches 390 °C. For the LI, region 2 for the 25% Al and Cu donor materials, the temperature is 480 and 391 °C, respectively, which is comparable to the temperature in the steel plate.

The temperature for the 25% Cu donor material in the RI, region 3 is consistent with the concept of the donor material for up to 7 s during the welding process, but the temperature unexpectedly starts to increase and reaches 583 °C at the 11 s mark. The temperature in the DS, region 4 is as expected in the Al, Cu donor materials as well in the 1045 steel plate, which is almost half of the temperature in the 1045 steel plate in the absence of either donor material. In Figure 9, the temperature in the three regions for the 50% Al and Cu donor

materials on the 1045 steel plate is measured as expected. The temperature in the steel plate in the absence of a donor material is higher than in the presence of a donor material in the LI, region 2, and RI, region 3 at 11 s, i.e., at the end of the welding process. The temperature in the DS, region 4 is comparable in all materials. In contrast to the 25% Cu donor material on the 1045 steel plate, the temperature rises as indicated above, but as the thickness increases to 50%, the effect disappears.

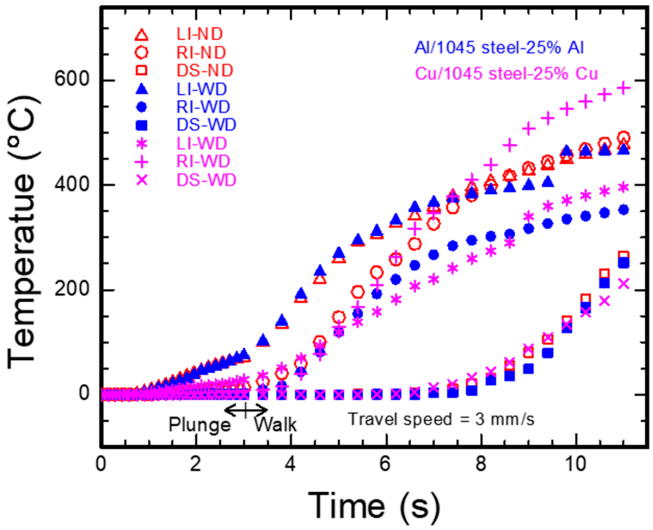

Figure 8. Temperature versus time. The red symbols represent the 1045 steel plate with no donor material. The blue symbols [LI, region 2 represents 25% Al donor material on the 1045 steel plate parent material, RI, region 3 represents the 1045 steel parent material, and DS, region 4 represents the 1045 steel parent material]. The pinky symbols [LI, region 2 represents 25% Cu donor material on the 1045 steel plate parent material, RI, region 3 represents the 1045 steel parent material, and DS, region 4 represents the 1045 steel parent material].

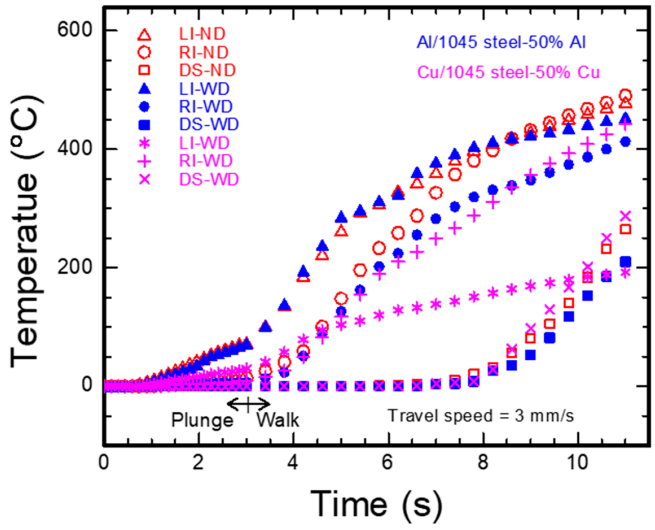

Figure 9. Temperature versus time. The red symbols represent the 1045 steel plate with no donor material. The blue symbols [LI, region 2 represents 50% Al donor material on the 1045 steel plate parent material, RI, region 3 represents the 1045 steel parent material, and DS, region 4 represents the 1045 steel parent material]. The pinky symbols [LI, region 2 represents 50% Cu donor material on the 1045 steel plate parent material, RI, region 3 represents the 1045 steel parent material, and DS, region 4 represents the 1045 steel parent material].

The plots of the axial force versus time during the plunge zone, region 1, are shown in Figure 10 for the Cu-Al donor/parent material and Figure 11 for Al and Cu donor materials

on 1045 steel plate. We notice that, upon the placement of the Cu donor material on the Al plate, there is a slight decrease in the forces at the end of the plunge, whereas there is a significant decrease in the forces in the 1045 steel plate regardless of the thickness of the donor material. The results of the axial force for the fine mesh in the 25% and 50% Cu donor material on the Al plate exhibited an enormous drop in the axial force in the plunge zone, as can be seen in Figure 9.

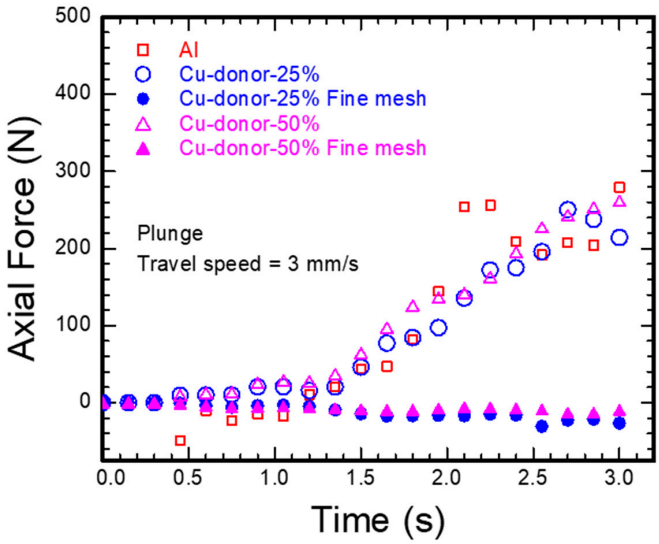

Figure 10. Axial force for the 25 and 50% Cu-Al donor/parent material in the plunge zone, region 1.

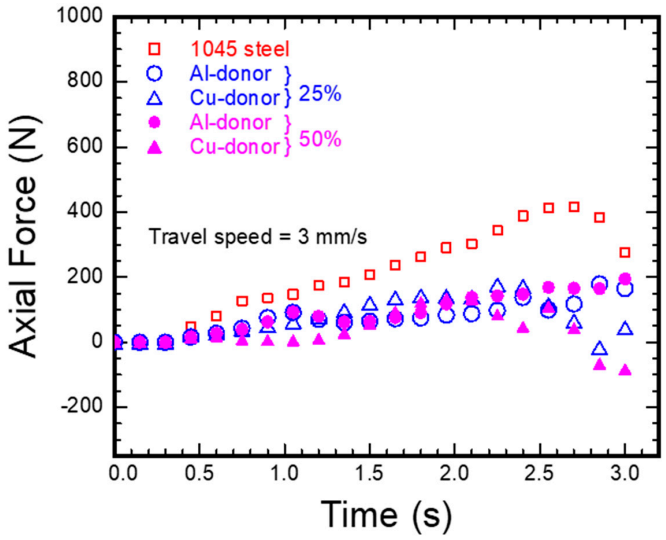

Figure 11. Axial force for the 25 and 50% Cu-Al donor materials on 1045 steel parent material in the plunge zone, region 1.

6. Comparison with Experiments

Experiments of the Cu-Al donor/base material combinations were conducted, and more details about the experiments could be found in [44]. While it took about 80 s to experimentally complete the welding of the aluminum plate, including the plunge and the walk stages, the simulation of the welding process lasted more than a day and a half to complete only 11 seconds of the simulations using the coarse mesh. The fine mesh model took more than two weeks to complete. To perform the simulation for 80 s using the coarse and fine meshes, it will probably take months to complete the simulation and it is not practical to do so. However, we decided to overlay the 11 s of the coarse and fine meshes onto the experimental results as shown in Figure 12. Both the coarse and fine mesh model

results agree well with the experimental results for the first 3 s during the plunge stage. The fine mesh model results continue to agree well with the experimental results during the welding stage for 2 more seconds, while the coarse mesh model results did not agree well with the experimental results. In general, both the coarse and fine mesh model results agree with the experimental results for the final 6 s during the welding stage. Therefore, we found it somehow feasible to compare the experiments and simulations results for only the 11 s of the simulations.

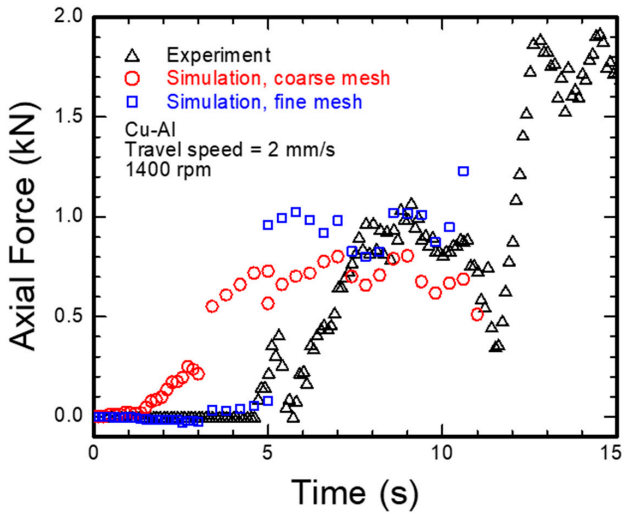

Figure 12. Compairson between the experimental and simualtion results of the axial force for the 25% Cu-Al donor/parent material.

7. Effect of Friction

In the simulations, using the new refined mesh model and a coefficient of friction of 0.3, 0.5, 0.7 and 1.0, we present the effect of the coefficient of friction on the temperature during the plunge stage. The temperature plot of the plunge zone versus time is shown in Figure 13. The temperature remains the same for up to 1.5 s. Temperature increases with increase in the coefficient of friction from 0.3 to 1.0. This takes place during 1.5 s until the end of the plunge stage at 3 s.

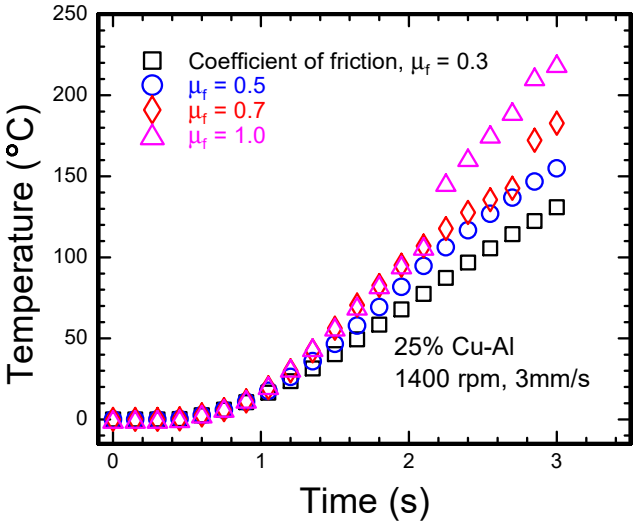

Figure 13. The effect of the coefficient of friction on the temperature for the 25% Cu-Al donor/parent material.

8. Conclusions

We conclude that Cu reduces the temperature significantly when used as a donor material for the Al plate in the plunge zone, region 1. The thickness of the Cu donor material has no significant impact when comparing the 25 or 50% Cu thickness.

We also conclude that Cu produced better results than Al as donor materials when used with 1045 steel plate during the plunge zone, Figures 3 and 4. The Cu donor material thickness of 25 or 50% produced similar results.

The temperature results in the LI, RI, and DS regions are consistent during the welding process for the 25 and 50% Cu donor material when used with the Al plate. Similarly, for the Al and Cu 25% donor materials when used with a 1045 steel plate, the temperature results are also consistent for all regions except for the Cu donor material in the RI region, and generally temperature increases past 7 s during the welding process. This effect disappears when the thickness of the donor material rises to 50%. Finally, we conclude that the axial force results are acceptable for the 25 and 50% Cu donor material when used with the Al plate. Similarly, Al and Cu donor materials, when used with the 1045 steel plate, reduced the axial forces compared to the axial forces in the 1045 steel plate with no donor material. This is expected to reduce the wear and tear in the tool head and prevent fracture of the tool head. A comparison between the simulation and experimental results revealed that the simulation and experimental results agree well with each other. The simulations were carried for only 11 s, whereas it took 80 s to complete the experiment.

Temperature increases with the increase in the coefficient of friction from 0.3 to 1.0 during the plunge stage from 1.5 to 3.0 s.

Author Contributions: Simulations, formal analysis, and validation, J.M. Review, editing, and experiments, S.B. Funding acquisition and project administration, Z.W. Conceptualization, supervision, and project administration, A.A.E. All authors have read and agreed to the published version of the manuscript.

Funding: This research was funded by NASA grant number 80NSSC20M0015.

Data Availability Statement: The data presented in this study are available upon request from the corresponding author.

Acknowledgments: The authors would like to acknowledge support from NASA (award number: 80NSSC20M0015). Any opinions, findings, and conclusions or recommendations expressed in this material are those of the author(s) and do not necessarily reflect the views of the NASA.

Conflicts of Interest: On behalf of all authors, the corresponding author states that there is no conflict of interest.

References

1. Thomas, W.M.; Nicholas, E.D.; Needham, J.C.; Murch, M.G.; Templesmith, P.; Dawes, C.J. Friction Stir Butt Welding. International Patent Application PCT/GB92/02203 and GB Patent Application 9125978.8, 6 December 1991.
2. Threadgill, P.L.; Leonard, A.J.; Shercliff, H.R.; Withers, P.J. Friction stir welding of aluminium alloys. *Int. Mater. Rev.* **2009**, *54*, 49–93. [CrossRef]
3. Haghshenas, M.; Gerlich, A.P. Joining of automative sheet materials by friction-based welding methods: A review. *Eng. Sci. Technol.* **2018**, *21*, 130–148.
4. Gerlich, A.; Su, P.; Yamamoto, M.; North, T.H. Effect of welding parameters on the strain rate and microstructure of friction stir spot welded 2024 aluminum alloy. *J. Mater. Sci.* **2007**, *43*, 2–11. [CrossRef]
5. North, T.H.; Bendzsak, G.J.; Gerlich, A.; Su, P.; Cingara, G. Transient local melting in Al 7075-T6 friction stir spot welds. *Mater. Sci. Forum* **2007**, *539*, 3826–3831. [CrossRef]
6. Ahmed, M.M.Z.; Jouini, N.; Alzahrani, B.; Seleman, M.M.E.-S.; Jhaheen, M. Dissimilar Friction Stir Welding of AA2024 and AISI 1018: Microstructure and Mechanical Properties. *Metals* **2021**, *11*, 330. [CrossRef]
7. Cabibbo, M.; Forcellese, A.; Santecchia, E.; Paoletti, C.; Spigarelli, S.; Simoncini, M. New Approaches to Friction Stir Welding of Aluminum Light-Alloys. *Metals* **2020**, *10*, 233. [CrossRef]
8. Wang, X.; Gao, Y.; McDonnell, M.; Feng, Z. On the solid-state-bonding mechanism in friction stir welding. *Extrem. Mech. Lett.* **2020**, *37*, 100727. [CrossRef]
9. Elrefaey, A.; Takahashi, M.; Ikeuchi, K. Friction stir welding of aluminum to zinc-coated steel. *J. Jpn. Weld. Soc.* **2005**, *23*, 186–193. [CrossRef]

10. Kimapong, K.; Watanabe, T. Friction stir welding of aluminum alloy to steel. *Weld. J.* **2004**, *83*, 277–282.
11. Thomas, W.M.; Nicholas, E.D. Friction stir welding for the transportation industries. *Mater. Des.* **1997**, *18*, 269–273. [CrossRef]
12. Mishra, R.S.; Ma, Z.Y. Friction stir welding and processing. *Mater. Sci. Eng. R* **2005**, *50*, 1–78. [CrossRef]
13. Mandal, S.; Rice, J.; Elmustafa, A.A. A Numerical Study of The Plunge StageFriction Stir Welding Using Abaqus. In *Friction Stir Welding and Processing IV, Proceedings of the 2007 TMS Annual Meeting & Exhibition, Orlando, FL, USA, 25 February–1 March 2007*; Mishra, R.S., Mahoney, M.W., Lienert, T., Jata, K.V., Eds.; Wiley: Hoboken, NJ, USA, 2007; pp. 127–133.
14. Thomas, W.M. Friction stir welding of ferrous materials—A feasibility study. In Proceedings of the First International Symposium on Friction Sir Welding, Thousand Oaks, CA, USA, 14–16 June 1999.
15. Thomas, W.M.; Nicholas, E.D.; Smith, S.D. *Friction Stir Welding-Tool Developments*; Minerals, Metals and Materials Society: Warrendale, PA, USA, 2001.
16. Lienert, T.J.; Stellwag, W.L., Jr.; Grimmett, B.B. Friction stir welding studies on mild steel. *Weld. J.* **2003**, *82*, 1–9. [CrossRef]
17. Mandal, S.; Williamson, K. A thermomechanical hot channel approach for friction stir welding. *J. Mater. Process. Technol.* **2006**, *174*, 190–194. [CrossRef]
18. Mandal, S.; Rice, J.; Elmustafa, A.A. Experimental and Numerical Investigation of the Plunge Stage in Friction Stir Welding. *J. Mater. Process. Technol.* **2008**, *203*, 411–419. [CrossRef]
19. Santella, M. Plunge testing to evaluate tool materials for friction stir welding of 6061 + 20wt% Al_2O_3 composite. In Proceedings of the 4th International Friction Stir Symposium, Park City, UT, USA, 14–16 May 2003.
20. Santella, M.L.; Engstrom, T.; Pan, T.-Y. Effects of friction stir processing on mechanical properties of the cast aluminum alloys A319 and A356. *Scripta Mater.* **2005**, *53*, 201–206. [CrossRef]
21. Gerlich, A.; Su, P. Numerical modeling of FSW spot welding: Preliminary results. In Proceedings of the 2006 TMS Annual Meeting, San Francisco, CA, USA, 13–17 February 2005.
22. Gerlich, A.; Su, P.; North, T.H. Tool penetration during friction stir spot welding of Al and Mg alloys. *J. Mater. Sci.* **2005**, *40*, 6473–6481. [CrossRef]
23. He, X.; Gu, F.; Ball, A. A review of numerical analysis of friction stir welding. *Prog. Mater. Sci.* **2014**, *65*, 1–66. [CrossRef]
24. Aval, H.J.; Serajzadeh, S.; Kokabi, A. Experimental and theoretical evaluations of thermal histories and residual stresses in dissimilar friction stir welding of AA5086–AA6061. *Int. J. Adv. Manuf. Technol.* **2012**, *61*, 149–160. [CrossRef]
25. Khosa, M.S.S.U. Thermo-mechanical investigations during friction stir spot welding (FSSW) of AA6082-T6. *Weld. World* **2010**, *54*, R134–R146. [CrossRef]
26. Mandal, S.; Rice, J.; Hou, G.; Williamson, K.W.; Elmustafa, A.A. Modeling and Simulation of a Donor Material Concept to Reduce Tool Wear in Friction Stir Welding of High-Strength Materials. *J. Mater. Eng. Perform.* **2013**, *22*, 1558–1564. [CrossRef]
27. Guerdoux, S.; Fourment, L. A 3D Numerical Simulation of Different Phases of Friction Stir Welding. *Modelling Simul. Mater. Sci. Eng.* **2009**, *17*, 075001. [CrossRef]
28. Assidi, M.; Fourment, L.; Guerdoux, S.; Nelson, T. Friction Model for Friction Stir Welding Process Simulation: Calibration from Welding Experiments. *Int. J. Mach. Tools Manuf.* **2010**, *50*, 143–155. [CrossRef]
29. Hossfeld, M. Modeling Friction Stir Welding: On Prediction and Numerical Tool Development. *Metal* **2022**, *12*, 1432. [CrossRef]
30. Hossfeld, M. Shoulderless Friction Stir Welding: A low-Force Solid State Keyhole Joining Technique for Deep Welding of Liable Structures. *Prod. Eng.* **2022**, *16*, 389–399. [CrossRef]
31. Hossfeld, M.; Roos, E. A New Approach to Modeling Friction Stir Welding Using the CEL Method. In Proceedings of the International Conference on Advanced Manufacturing Engineering and Technologies, Stockholm, Sweden, 27–30 October 2013.
32. Rice, J.; Mandal, S.; Elmustafa, A.A. Microstructural investigation of donor material experiments in friction stir welding. *Int. J. Mater. Form* **2014**, *7*, 127–137. [CrossRef]
33. Schmidt, H.; Hattel, J. A local model for the thermomechanical conditions in friction stir welding. *Model. Simul. Mater. Sci Eng.* **2005**, *13*, 77–93. [CrossRef]
34. Johnson, G.R.; Cook, W.H. Fracture Characteristics of Three Metals Subjected to Various Strains, Strain Rates, Temperatures and Pressures. *Eng. Fract. Mech.* **1985**, *21*, 31–48. [CrossRef]
35. Jaspers, S.P.F.C.; Dautzenberg, J.H. Material Behaviour in Conditions Similar to Metal Cutting: Flow Stress in the Primary Shear Zone. *J. Mater. Process. Technol.* **2002**, *122*, 322–330. [CrossRef]
36. *ABAQUS*; Version 6.20; Simulia: Johnston, RI, USA, 2018.
37. Grujicic, M.; Arkere, G.; Pandurangan, B.; Ochterbeck, J.M.; Yen, C.-F.; Cheeseman, B.A.; Reynolds, A.P.; Sutton, M.A. Computational analysis of material flow during friction stir welding of AA5059 aluminum alloys. *J. Mater. Eng. Perform.* **2012**, *21*, 1824–1840. [CrossRef]
38. Meyghani, B.; Awang, M.; Wu, C. Thermal analysis of friction stir welding with a complex curved welding seam (technical note). *Int. J. Eng. Trans. A Basics* **2019**, *32*, 1480–1484. [CrossRef]
39. Frigaard, O.; Grong, O.; Midling, T. A Process Model for Friction Stir Welding of Age Hardening Aluminum Alloys. *Metal. Mater. Transit. A* **2001**, *32*, 1189–1200. [CrossRef]
40. Soundararajan, V.; Zekovic, S.; Kovacevic, R. Thermo-Mechanical Model with Adaptive Boundary Conditions for Friction Stir Welding of Al AA6061. *Int. J. Mach. Tools Manuf.* **2005**, *45*, 1577–1587. [CrossRef]
41. JI, S.-D.; Liu, J.-G.; Yue, Y.-M.; Zan, L.; Li, F. 3d numerical analysis of material flow behavior and flash formation of 45# steel in continuous drive friction welding. *Trans. Nonferrous Met. Soc. China* **2012**, *22*, S528–S533. [CrossRef]

42. Nimesh, P. Simulation of inertia friction welding of mild steel and aluminum 6061 using finite element method on abaqus. *IJAPIE* **2016**, *1*, 29–39.
43. Lambiase, F.; Paoletti, A.; Di Ilio, A. Forces and temperature variation during friction stir welding of aluminum alloy AA6082-T6. *Int. J. Adv. Manuf. Technol.* **2018**, *99*, 337–346. [CrossRef]
44. Bhukya, S.N.; Wu, Z.; Maniscalco, J.; Elmustafa, A.A. Effect of copper donor material-assisted friction stir welding of AA6061-T6 alloy on downward force, microstructure, and mechanical properties. *Int. J. Adv. Manuf. Technol.* **2022**, *119*, 2847–2862. [CrossRef]